

Published in final edited form as:

Cancer Res. 2015 January 1; 75(1): 194–202. doi:10.1158/0008-5472.CAN-13-3131.

Contributions to drug resistance in glioblastoma derived from malignant cells in the sub-ependymal zone

Sara GM Piccirillo^{1,†}, Inmaculada Spiteri^{#2}, Andrea Sottoriva^{#2,3}, Anestis Touloumis^{2,4}, Suzan Ber¹, Stephen J Price⁵, Richard Heywood¹, Nicola-Jane Francis⁶, Karen D Howarth⁷, Vincent P Collins⁸, Ashok R Venkitaraman⁶, Christina Curtis³, John C Marioni⁴, Simon Tavaré², and Colin Watts^{1,5,†}

¹John van Geest Centre for Brain Repair, Department of Clinical Neurosciences, University of Cambridge, Cambridge, UK

²Cancer Research UK Cambridge Institute, Li Ka Shing Centre, Cambridge, UK

³Department of Preventive Medicine, Keck School of Medicine, University of Southern California, Los Angeles, California, USA

⁴European Bioinformatics Institute (EMBL-EBI), Wellcome Trust Genome Campus, Hinxton, Cambridge, UK

⁵Division of Neurosurgery, Department of Clinical Neurosciences, University of Cambridge, Addenbrooke's Hospital, Cambridge, UK

⁶Department of Oncology and the Medical Research Council Cancer Cell Unit, Hutchison/MRC Research Centre, Cambridge, UK

⁷Hutchison/MRC Research Centre and Department of Pathology, University of Cambridge, Cambridge, UK

⁸Division of Molecular Histopathology, Department of Pathology, University of Cambridge, Addenbrooke's Hospital, Cambridge, UK

These authors contributed equally to this work.

Abstract

[†]To whom correspondence should be addressed. sp577@cam.ac.uk (S.G.M.P.); cw209@cam.ac.uk (C.W.).

Author Contributions

S.G.M.P. designed and performed the experiments, collected, analyzed and interpreted the data and wrote the manuscript. I.S. performed experiments, collected, analyzed and interpreted the data and contributed to manuscript preparation. A.S. contributed to the design of the tissue multi-sampling scheme for phylogeny, analyzed and interpreted the data and contributed to manuscript preparation. A.T. contributed to data analysis. S.B. performed experiments. S.J.P. provided tissue samples. R.H. collected tissue samples. N.F. reviewed and edited the manuscript. K.D.H. performed experiments. V.P.C. performed histopathological analysis, reviewed and edited the manuscript. A.R.V. reviewed and edited the manuscript. C.C. generated and interpreted the data, reviewed and edited the manuscript. J.C.M. reviewed and edited the manuscript. S.T. designed the overall study, supervised the project, interpreted the data and edited the manuscript. C.W. designed the overall study, supervised the project, provided tissue samples, contributed to the design of the tissue multi-sampling scheme for phylogeny, interpreted the data and edited the manuscript. All authors discussed the results and commented on the manuscript.

Disclosure of conflicts of interest

The authors disclose no potential conflicts of interest.

Author Information

The data reported in this paper are deposited in ArrayExpress (accession codes E-MTAB-1129 and E-MTAB-1215).

Glioblastoma (GB), the most common and aggressive adult brain tumor, is characterized by extreme phenotypic diversity and treatment failure. Through fluorescence-guided resection, we identified fluorescent tissue in the sub-ependymal zone (SEZ) of GB patients. Histological analysis and genomic characterization revealed that the SEZ harbors malignant cells with tumor-initiating capacity, analogous to cells isolated from the fluorescent tumor mass (T). We observed resistance to supra-maximal chemotherapy doses along with differential patterns of drug response between T and SEZ in the same tumor. Our results reveal novel insights into GB growth dynamics, with implications for understanding and limiting treatment resistance.

Introduction

The basis of phenotypic diversity and treatment failure in human GB is poorly understood. Murine models of gliomagenesis point to sub-ependymal neural stem cells (NSCs) as a putative cell of origin for astrocytic tumors. The stepwise pre-malignant loss of tumor suppressors p53, NF1 & PTEN (1, 2) has been shown to lead to the development of an aggressive disease characterized by resistance to genotoxic injury (3).

Additionally, stratifying patients using transcriptional profiles derived from a large cohort of GB single tumor samples (4) has identified multiple disease subtypes, which may have prognostic significance (5, 6). However, emerging data on genomic intra-tumor heterogeneity in GB indicate spatial segregation of genetically distinct clones in the same tumor (7), making the interpretation of single-sample tumor data challenging. Importantly, this may contribute to the pervasive failure of treatment in GB patients.

Clinical trials have established that use of a fluorescence biomarker, 5-aminolevulinic acid (5-ALA), can enhance the surgical resection of GB (8). We have demonstrated the use of 5-ALA in a Fluorescence-Guided Multiple Sampling (FGMS) strategy that permits real-time spatially segregated tumor sampling during surgery (7, 9). Combining visible fluorescence with neuroanatomy allows for the objective distinction of the tumor mass T (visible fluorescent). Importantly, a spatially distinct and visibly fluorescent sub-ependymal zone (SEZ) can also be identified in a subset of GB patients.

Here we report an integrated genomic analysis of SEZ and T samples, obtained by FGMS, which reveals that malignant cells in the SEZ contribute to tumor growth. Functional characterization confirms that the SEZ contains tumor-initiating cells (TICs) that can recapitulate the disease in orthotopic patient-derived xenogeneic models in a manner similar to TICs isolated from the corresponding T. TICs in the SEZ contribute to resistance to chemotherapy and show differential patterns of response when compared to T of the same patients.

Materials and Methods

GB sample collection

Patient informed consent was obtained through our research clinic (10). Tissue collection protocols were compliant with the UK Human Tissue Act 2004 (HTA Licence ref 12315) and approved by the Local Regional Ethics Committee (LREC ref 04/Q0108/60). No

difference in 5-ALA labeling capacity was observed among patients. See Supplementary Experimental Procedure for details on 5-ALA administration and sample collection.

Quantitative Real-time PCR analysis

Total RNA was extracted from T and SEZ tissues using TRIzol (Invitrogen) according to the manufacturer's instructions. RNA was treated with DNase (Qiagen) and cDNA was synthesized from 5 μ g of total RNA using Random Primers (Invitrogen) and a Superscript III First-Strand Synthesis System for real-time PCR (RT-PCR) (Invitrogen). The RT-PCR for *Nestin*, *Gfap*, *Sox2* and *MIB1* transcripts was performed using CFX96 RT-PCR (Biorad), RT² qPCR Primer Assay and SYBR Green Master Mix (Qiagen) according to the manufacturer's instructions. 18S was used as the housekeeping reference. Relative expression quantification was performed by the $\Delta\Delta$ CT method. Experiments were performed in triplicate and each experiment was repeated 3 times.

Cell line derivation and implantation

Cell cultures from T and SEZ of 42 patients were established from GB patients undergoing surgery at Addenbrooke's Hospital, Cambridge, in 2010-2012. The cells were isolated as described (9, 11, 12) and used either uncultured (primary) or propagated *in vitro* for 2 passages (briefly cultured) in serum-free medium. The U87 cell line was obtained from the American Type Culture Collection, cultured according to the supplier's recommendations and used just after resuscitation. Tissue collection to establish HFNSCs was approved by the Local Regional Ethics Committee. Cells were established in 2011 and grown in serum-free medium in order to form neurospheres and used at early passage. All the cell cultures have been tested for mycoplasma contamination by PCR before use. See Supplementary Experimental Procedure for details on cell propagation, immunofluorescence and *in vivo* experiments.

DNA and RNA extraction

DNA from T and SEZ tissues of 14 GB patients was extracted for copy number analysis using DNeasy Blood & Tissue Kit (Qiagen). RNA from T and SEZ tissues of 15 GB patients was extracted for gene expression analysis using Trizol (Invitrogen) and cleaned up using MiniElute columns (Qiagen). See Supplementary Experimental Procedure for details on copy number and gene expression analysis. Copy number results were validated by fluorescence in situ hybridization as described in the Supplementary Experimental Procedure.

Drug treatment assay

Treatment with Temozolomide, Cisplatin and Cediranib was evaluated using the *in vitro* BrdU cell proliferation assay (Millipore). 3 \times 10³ cells were plated in triplicate per treatment condition. Control wells for Temozolomide, Cisplatin and Cediranib are shared as these treatments have been applied in the same experiments. One day after plating, the treatment was applied for 3 days. BrdU was applied in the final 24 hours of the treatment. Each experiment was repeated 3 times. See Supplementary Experimental Procedure for details on drug concentration.

MGMT promoter methylation

Analysis of MGMT promoter methylation was performed by PCR (13) and by pyrosequencing (14). In brief, DNA was bisulfite converted and subsequently subjected to PCRs using specific primer pairs for the methylated or the modified unmethylated DNA. PCR products were resolved in a 2% agarose gel stained with SybrSafe. See Supplementary Experimental Procedure for further details.

Phylogenetic reconstruction

Multiple spatially separated samples taken from each GB were collected in order to reconstruct the phylogenetic relationship between the tumor and the SEZ using copy number profiles and molecular clock analysis. See Supplementary Experimental Procedure for further details.

Statistical analysis

For *in vivo* experiments using Nod/Scid animals, we performed Kaplan-Meier survival analysis using the Logrank test for hypothesis testing.

For drug response analysis using BrdU, a one-way ANOVA was performed for each patient.

The *p*-values for the pairwise mean comparisons of each treatment to the corresponding control were calculated using Tukey's Honestly Significant Difference test. In the related figures and for each patient, we plotted the normalized mean treatment response using the corresponding mean control as a reference, except in Supplementary Fig. 12, where we normalized to the mean of the 50 μ M TMZ treatment response. The minimum and maximum normalized values are provided in order to present the dispersion of the normalized data.

Results

SEZ harbors residual disease in GB patients

We screened 65 GB patients given 5-ALA and confirmed that visibly fluorescent disease extended to the SEZ in 65% (42/65) of the cases. Multiple samples were obtained from 14 patients. Histological features of high-grade glioma (15) were detected in SEZ and T of the patients (Fig. 1A; additional two representative GBs are shown in Supplementary Fig. S1, A and B). SEZ tissue was also used to identify the ependymal layer and confirm correct sampling (Supplementary Fig. S2).

GB has been shown to heterogeneously express glial fibrillary acidic protein (Gfap) (16) and consistent with this we noted high expression of Gfap in SEZ samples compared to matched T samples (Fig. 1, B and C top panel and Supplementary Fig. S1C). Expression of the precursor marker Nestin was detected both in T and SEZ tissues (Fig. 1, B and C middle panel and Supplementary Fig. S1C). The SEZ showed increased vascularization in comparison to T, as determined by CD31 expression (Fig. 1, B and C bottom panel). Weak expression of the neuronal marker Tuj1 was observed in both areas (Supplementary Fig. S1C). One of the histological hallmarks of GB is high proliferative activity (17) and we observed similar numbers of mitotic cells in T and SEZ (MIB1 index 20.5 \pm 2.8 and 18.1 \pm 1.9

respectively) (Supplementary Fig. S1C). The extent of focal necrosis was similar in T and SEZ of the same patients (except for sp40) (Supplementary Table S1). Consistent with immunohistochemical analysis, T and SEZ contained similar amounts of tumor tissue (except for sp54) (Supplementary Table S1). Together these data suggest that regulatory mechanisms promoting proliferation and vascularization are common to the T and the SEZ tissues.

To confirm these findings we performed real-time analysis of gene expression for markers of glial and precursors cells (*Gfap* and *Nestin*), stem cells (*Sox2*), proliferation (*MIB1*) on T and SEZ tissues of 3 GBs in total (Supplementary Fig. S3). Our results show increased expression of *Gfap* in the SEZ compared with the corresponding T (Supplementary Fig. S3). The expression of *Nestin* and *Sox2* is similar between T and SEZ, except in sp10 for *Sox2* (Supplementary Fig. S3).

We applied high-throughput genomic profiling techniques to the SEZ and T to characterize each of these regions. DNA/RNA were extracted from the tissues of the 14 patients (Supplementary Table S2A). After quality assessment, we analyzed copy number aberrations (CNAs) of 8 patients and gene expression profiles of 9 patients (6 of whom were common to both analyses) (Supplementary Table S2B shows the patient clinical information). Our data reveal multiple aberrations (e.g. EGFR amplification and CDKN2A deletions) common to T and the corresponding SEZ in individual patients (Fig. 2A and Supplementary Fig. S4). In 6/8 patients, the SEZ had an equal or smaller number of putative driver aberrations with respect to the corresponding T (mean difference in the number of aberrations is 1.27 ± 0.38 ; p -value = 0.12). CNA results were validated by fluorescence in situ hybridization (FISH) for three GB drivers, EGFR, MET and PTEN (4), in three patients with available tissue (Fig. 2B and Supplementary Fig. S5, A-H). Because we observed *in vitro* aberrations in the corresponding cell cultures (Supplementary Fig. S6), we restricted further genomic analysis to tissue samples.

Clustering of the gene expression data (18) revealed that only 3/9 paired samples (SEZ and T from the same patient) clustered tightly together while 5/9 SEZ were assigned to the same sub-cluster, suggesting a SEZ-specific expression profile across patients (Fig. 2C).

We used a previously published classifier to assign our samples into one of 4 GB subtypes (6). 7/9 SEZ were classified as Mesenchymal (sp41, sp42, sp52, sp54, sp56, sp57 and r4) and the remaining 2 were Classical (sp49 and sp55). For 6/9 patients the SEZ was assigned to a different subtype than the corresponding T. T samples were distributed amongst the 4 subtypes (Classical, Mesenchymal, Neural and Proneural) (Fig. 2D).

We next investigated whether gene expression levels differed between SEZ and T. We rejected the hypotheses of no significant differences in the expression levels of all genes between SEZ and T (p -value < 0.00001), which suggests that there are differentially expressed genes in SEZ and T.

We next used the R package HDTD to identify gene ontology (GO) terms whose genes are differentially expressed (Supplementary Table S3).

Tumor-initiating cells reside in the SEZ

We next extended the characterization of T and SEZ to TIC populations. In neuro-epithelial malignancies the purification of TICs remains challenging because no robust cell-surface marker has been identified to distinguish tumorigenic and non-tumorigenic cells (19, 20). Initial data identifying CD133/Prominin1 as a marker in human GB (21) were subsequently challenged both in primary and cultured TICs (reviewed in (19)). More recently the cell surface marker CD15/SSEA-1 has been identified as a possible TIC marker in GB and medulloblastoma (22, 23). CD15 is a carbohydrate moiety expressed by neural stem and progenitor cells (24) but its use as GB marker did not find additional confirmation (25).

We therefore used a marker-independent approach (9, 11, 12, 26) to isolate cells from T and SEZ under serum-free conditions *in vitro* (Fig. 3A). Growth curve analysis and limiting-dilution assays confirmed long-term self-renewal and expansion (Fig. 3B and Supplementary Fig. S7), clonogenicity and multipotency similar to the corresponding T cells (Supplementary Fig. S8).

We evaluated the expression of the precursor marker Nestin and other putative TIC markers (A2B5, CD133, CD15) from T and SEZ (reviewed in (19)) and found similar expression of Nestin in T and SEZ cells, in agreement with the data in Fig. 1, B and C. In contrast, A2B5-, CD133- and CD15-positive cells were rarely found (Supplementary Fig. S9, A and B).

Despite phenotypic differences *in vitro*, orthotopic inoculation of T and SEZ cells in NOD-SCID mice consistently generated tumors in all cases (Fig. 3, C and D and Supplementary Fig. S10). Nonetheless, a statistically significant shorter survival was observed for animals injected with T cells compared to those injected with SEZ cells (Fig. 3C and Supplementary Fig. S10; p -value <0.05).

To our knowledge, this is the first time that SEZ cells from GB patients have been tested for their tumorigenic potential. We analyzed the *in vivo* properties of enriched SEZ cells from 3 additional GBs. In all cases SEZ cells gave rise to tumors with similar patterns of growth and infiltration to those generated from TICs isolated from T under the same experimental conditions (Supplementary Fig. S11, A-C).

TICs from the SEZ contribute to drug resistance

The SEZ and T contained self-renewing TICs suitable for chemo-response assays. These cells are grown in conditions that better preserve the genotype of the original disease (27) and have been proposed for use in high-throughput drug screening (28, 29). We tested the effects of the oral alkylating agent Temozolomide (TMZ), the current standard of care in GB patients (30). To facilitate analysis, we assayed methylation in the promoter region of MGMT, a methyltransferase that inhibits the cytotoxic effect of TMZ and is a predictive biomarker in GB (31).

We initially treated TICs isolated from T and SEZ of 7 GB patients with TMZ at maximum concentrations reported for the brain and plasma (50 μ M) (32, 33), but no significant treatment response was observed relative to the corresponding controls (vehicle only). Only sp12 showed a significant response in both T and SEZ (Supplementary Fig. S12). We

therefore analyzed a set of TICs isolated from T of 20 patients using a dose escalation strategy ranging from 50 μ M to 2.5mM of TMZ, and found that only 20% of the samples exhibited a significant response at 500 μ M (Supplementary Fig. S13, A and B).

Based on these results we performed cell proliferation assays for TMZ concentrations between 50 μ M and 2.5mM on TICs isolated from T and SEZ of the same tumor for 8 patients. We noted that TICs continued to proliferate in the SEZ and T at supra-maximal drug concentrations. We also observed that the response varied between T and SEZ of the same GB (Fig. 4A and Supplementary Fig. S14A). Three patterns emerged: differential response between T and SEZ (e.g. sp13, sp20, sp37 and sp42), both T and SEZ respond (e.g. sp17, sp23), neither T nor SEZ respond (e.g. sp14, except at 2.5 mM TMZ for T, and sp52).

To test whether resistance to TMZ was MGMT-dependent, we analyzed the DNA methylation status of the MGMT promoter by pyrosequencing (Supplementary Table S4) and methylation-specific PCR (13) (Supplementary Fig. S15) and we found that the results were in agreement except for sp42.

Our PCR analysis revealed that 4/7 paired TICs (sp14, sp23, sp37 and sp52) did not show methylation of the MGMT promoter in either the T or the SEZ consistent with the poor response to TMZ, except for sp23 (T and SEZ) and sp37T. In contrast, sp17, sp20 and sp42 are methylated and showed a better response to TMZ among all the tested TICs with the exception of sp20SEZ and sp42T (Fig. 4A and Supplementary Fig. S14A). All together, our results suggest that MGMT methylation status is homogeneous in T and SEZ of the same patients and generally predicts response to TMZ (Supplementary Table S5).

We also evaluated the anti-mitotic agent Cisplatin, previously used in GB therapy, and Cediranib, an anti-angiogenic inhibitor of VEGFRs with additional activity against PDGFRs, recently used in clinical trials (34, 35) (Fig. 4B and Supplementary Fig. S14B). Although anti-angiogenic therapies target the endothelial compartment, it has been reported that VEGFRs are enriched on the surface of TICs from GB (36). VEGF signals via its endothelial tyrosine kinase receptor 2 (VEGFR2) (35), so we first confirmed that this receptor is expressed in TICs from T and SEZ (Supplementary Fig. S16). We next quantified the expression of VEGF and PDGF receptors. No significant difference was present between T and SEZ (no VEGFR1 nor VEGFR3 probe was available in the Illumina arrays) (Supplementary Table S6).

Exposure to Cisplatin and Cediranib revealed resistant TICs in T and SEZ together with a heterogeneous response profile (Fig. 4B and Supplementary Fig. S14B). Whereas sp17 and sp23 showed sensitivity to these treatments in T and SEZ, a significant response was observed only in one of the two regions for sp13, sp20 and sp52 (Fig. 4B).

The drug response profile of TICs from T and SEZ of the same patients emphasizes their potential utility in drug development compared to standard glioma cell lines e.g. U87 and human fetal neural stem cells (HFNSCs). U87 significantly responded to treatment with TMZ, Cisplatin and Cediranib whereas two HFNSCs lines (HFNSC and HFNSC1) were resistant to TMZ, as previously reported (37) and to Cisplatin and Cediranib (Supplementary Fig. S17).

Phylogenetic reconstruction suggests different patterns of GB evolution involving SEZ malignant cells

Our genomic and chemo-response assays data show that the SEZ harbors malignant cells that contribute to tumor growth and murine models of GB indicate that the SEZ is enriched for tumor ancestors (2, 38-40). However, this has not been confirmed in GB patients. We analyzed SEZ and T samples to determine if tumor cells grow out of the SEZ or into the SEZ. We reconstructed tumor ancestral trees in 8 patients, using several genomic measurements derived from multiple spatially separated samples taken from the GB mass (T1-T6) and SEZ. We have previously employed this approach to describe intra-tumor heterogeneity in T and infer tumor evolution (7) and we now used FGMS to position the SEZ. In particular, we reconstructed phylogeny based on genome-wide DNA copy number (41). In an independent assay, we exploited the observation that cells record their ancestral history in the form of neutral DNA methylation patterns (42, 43). This analysis is not biased by the presence of non-neoplastic cells as only highly proliferative tissues accumulate sufficient methylation events (tumors and colonic epithelium) (44) (Fig. 5A). We first validated the molecular clock loci chosen for this analysis (Fig. 5, B and C, top) and then calculated the normal cell content in SEZ and T. The values of cellularity indicate no significant difference (Fig. 5, B and C, bottom).

These orthogonal techniques yielded highly concordant phylogenies: in sp52, sp54, sp56 and sp57, the SEZ harbors tumor precursor cells that gave rise to the GB mass (Fig. 5D). In sp42 and sp49, we observed a similar trend although the two methods are not in full agreement (Fig. 5D). Analysis of sp55 and sp58 suggests a different pattern of evolution and emphasizes the heterogeneous nature of GB (Fig. 5D). Taken together, these data suggest that the SEZ contains a reservoir of malignant cells that are either tumor precursor clones or clones generated during GB evolution.

Discussion

Our comprehensive phenotypic, genomic and functional analysis reveals residual disease in the SEZ of GB patients (Fig. 1A and Supplementary Fig. S1, A and B). TICs are present in T and SEZ of the same GBs (Fig. 3C and Supplementary Fig. S10) and show differential patterns of therapeutic responsiveness and drug resistance (Fig. 4, A and B and Supplementary Fig. S14, A and B), suggesting that the SEZ should be considered as a novel potential therapeutic target in a subset of GB patients. This is confirmed by phylogenetic reconstruction showing different patterns of tumor evolution with the SEZ harboring precursor clones or clones generated during the GB growth (Fig. 5D).

Gene expression profiling of SEZ reveals that different GB subtypes (6) are present within the same patient. The SEZ is predominantly Mesenchymal (7 patients) or Classical (2 patients). T is more diverse, with representation from all four subtypes (Fig. 2D). Thus it is possible to envisage a spectrum of expression patterns with Mesenchymal/Classical representing proliferative diversification at the tumor core.

Previous reports suggested that proximity to the SEZ predicts a multifocal tumor phenotype and recurrences that arise at locations distant from the initial lesion (45). More recently it

has also been reported that contact of the tumor mass with the SEZ correlates with shorter survival (46). To explore this, we isolated TICs from T and SEZ of the same patients. TICs have been described in human GB but no analysis based on FGMS has been performed. Our results show that *in vivo* both T- and SEZ-derived cells generated tumors, however cells from T are more tumorigenic in comparison to the SEZ in agreement with the CNAs of the patient samples showing a trend towards a smaller number of aberrations in the SEZ. These data suggest that the tumorigenic potential is exacerbated when increased genetic alterations are acquired by the cancer genome in line with previous reports (47, 48).

Since genomic and phenotypic analyses suggest that the SEZ harbors tumor cells, it is crucial to investigate whether there are differences in response to therapy in cells isolated from this region. It has been previously shown that patient-derived TICs accurately represent parent disease (27) and have potential application in high-throughput drug screening (28, 29). Our data reveal that TICs from T and SEZ of the same GBs show different patterns of response to therapies that represent the current standard of care (Fig. 4, A and B, Supplementary Fig. S14, A and B and Supplementary Table S5). This suggests that they should be targeted using different approaches. Our results also reveal that a clinically significant fraction of cells is resistant to current treatments. This is consistent with murine data (3) indicating that multi-modal stratified approaches will be essential to improve therapeutic responsiveness.

GB evolves by following poorly understood spatial and temporal dynamics arising from cells of origin that are yet to be defined. The presence of malignant cells in the SEZ suggests two different scenarios of evolution with the GB growing into the SEZ or out of this region. Our phylogenetic data indicate that in 4/8 patients a pool of malignant precursor clones evolved in the SEZ (Fig. 5D). Given the presence of neural stem cells in the adult human SEZ (49), it has been suggested that GB is derived from those cells (50). This concept has been investigated in mouse models (2, 38-40), but until now there has been no direct evidence of the contribution of SEZ cells in human gliomagenesis. We show that the SEZ is a reservoir of disease and could be targeted therapeutically. Consistent with this, preliminary evidence suggest that irradiation of the SEZ in GB patients is associated with improved progression-free survival (51, 52).

In summary, we present a phenotypic, genomic and functional analysis of residual disease in human GB (Supplementary Fig. S18, A and B). Our approach together with FGMS provides a coherent strategy for interrogating the mechanistic basis of clinical heterogeneity in future studies. This is likely to further refine our understanding of the complex molecular landscape of GB, resulting in improved therapeutic strategies specifically aimed at targeting the SEZ.

Supplementary Material

Refer to Web version on PubMed Central for supplementary material.

Acknowledgments

We thank Amy Frary for tissue collection, Andy Lynch for help with the design of the expression array layout, Danita Pearson and Suet-Feung Chin for assistance in FISH, Cancer Research UK Cambridge Institute Genomics core facility for processing the Illumina arrays and Paul Edwards for comments during manuscript preparation. We acknowledge the Human Research Tissue Bank and Biomedical Research Centre for the tissue being accessed through the Human Research Tissue Bank. The Human Research Tissue Bank is supported by the NIHR Cambridge Biomedical Research Centre.

Financial support

This study was supported by the Addenbrooke's Charitable Trust; the National Institute for Health Research Cambridge Biomedical Research Centre; the Higher Education Funding Council for England; the Royal College of Surgeons of Edinburgh; the European Commission-Seventh Framework Programme (Marie Curie Intra-European Fellowship to S.G.M.P.); Cancer Research UK Programme Grant C14303/A10825 (S.T., I.S., A.S.) and C1023/A14545 (K.D.H.); EBI funding (A.T., J.C.M); University of Southern California (C.C.).

References

1. Zhu Y, Guignard F, Zhao D, Liu L, Burns DK, Mason RP, et al. Early inactivation of p53 tumor suppressor gene cooperating with NF1 loss induces malignant astrocytoma. *Cancer Cell*. 2005; 8:119–30. [PubMed: 16098465]
2. Alcantara Llaguno S, Chen J, Kwon CH, Jackson EL, Li Y, Burns DK, et al. Malignant astrocytomas originate from neural stem/progenitor cells in a somatic tumor suppressor mouse model. *Cancer Cell*. 2009; 15:45–56. [PubMed: 19111880]
3. Chen J, Li Y, Yu TS, McKay RM, Burns DK, Kernie SG, et al. A restricted cell population propagates glioblastoma growth after chemotherapy. *Nature*. 2012; 488:522–6. [PubMed: 22854781]
4. Cancer Genome Atlas Research Network. Comprehensive genomic characterization defines human glioblastoma genes and core pathways. *Nature*. 2008; 455:1061–8. [PubMed: 18772890]
5. Phillips HS, Kharbanda S, Chen R, Forrest WF, Soriano RH, Wu TD, et al. Molecular subclasses of high-grade glioma predict prognosis, delineate a pattern of disease progression, and resemble stages in neurogenesis. *Cancer Cell*. 2006; 9:157–73. [PubMed: 16530701]
6. Verhaak RG, Hoadley KA, Purdom E, Wang V, Qi Y, Wilkerson MD, et al. Integrated genomic analysis identifies clinically relevant subtypes of glioblastoma characterized by abnormalities in PDGFRA, IDH1, EGFR, and NF1. *Cancer Cell*. 2010; 17:98–110. [PubMed: 20129251]
7. Sottoriva A, Spiteri I, Piccirillo SG, Touloumis A, Collins VP, Marioni JC, et al. Intratumor heterogeneity in human glioblastoma reflects cancer evolutionary dynamics. *Proc Natl Acad Sci U S A*. 2013; 110:4009–14. [PubMed: 23412337]
8. Stummer W, Pichlmeier U, Meinel T, Wiestler OD, Zanella F, Reulen HJ. Fluorescence-guided surgery with 5-aminolevulinic acid for resection of malignant glioma: a randomised controlled multicentre phase III trial. *The lancet oncology*. 2006; 7:392–401. [PubMed: 16648043]
9. Piccirillo SG, Dietz S, Madhu B, Griffiths J, Price SJ, Collins VP, et al. Fluorescence-guided surgical sampling of glioblastoma identifies phenotypically distinct tumour-initiating cell populations in the tumour mass and margin. *Br J Cancer*. 2012; 107:462–8. [PubMed: 22722315]
10. Guilfoyle MR, Weerakkody RA, Oswal A, Oberg I, Jeffery C, Haynes K, et al. Implementation of neuro-oncology service reconfiguration in accordance with NICE guidance provides enhanced clinical care for patients with glioblastoma multiforme. *Br J Cancer*. 2011; 104:1810–5. [PubMed: 21610702]
11. Piccirillo SG, Combi R, Cajola L, Patrizi A, Redaelli S, Bentivegna A, et al. Distinct pools of cancer stem-like cells coexist within human glioblastomas and display different tumorigenicity and independent genomic evolution. *Oncogene*. 2009; 28:1807–11. [PubMed: 19287454]
12. Fael Al-Mayhany TM, Ball SL, Zhao JW, Fawcett J, Ichimura K, Collins PV, et al. An efficient method for derivation and propagation of glioblastoma cell lines that conserves the molecular profile of their original tumours. *J Neurosci Methods*. 2009; 176:192–9. [PubMed: 19215724]

13. Esteller M, Hamilton SR, Burger PC, Baylin SB, Herman JG. Inactivation of the DNA repair gene O6-methylguanine-DNA methyltransferase by promoter hypermethylation is a common event in primary human neoplasia. *Cancer Res.* 1999; 59:793–7. [PubMed: 10029064]
14. Malley DS, Hamoudi RA, Kocalkowski S, Pearson DM, Collins VP, Ichimura K. A distinct region of the MGMT CpG island critical for transcriptional regulation is preferentially methylated in glioblastoma cells and xenografts. *Acta Neuropathol.* 2011; 121:651–61. [PubMed: 21287394]
15. Louis DN, Ohgaki H, Wiestler OD, Cavenee WK, Burger PC, Jouvet A, et al. The 2007 WHO classification of tumours of the central nervous system. *Acta Neuropathol.* 2007; 114:97–109. [PubMed: 17618441]
16. Reifenberger G, Collins VP. Pathology and molecular genetics of astrocytic gliomas. *J Mol Med (Berl).* 2004; 82:656–70. [PubMed: 15316624]
17. Karamitopoulou E, Perentes E, Diamantis I, Maraziotis T. Ki-67 immunoreactivity in human central nervous system tumors: a study with MIB 1 monoclonal antibody on archival material. *Acta Neuropathol.* 1994; 87:47–54. [PubMed: 7511316]
18. Saeed AI, Bhagabati NK, Braisted JC, Liang W, Sharov V, Howe EA, et al. TM4 microarray software suite. *Methods Enzymol.* 2006; 411:134–93. [PubMed: 16939790]
19. Piccirillo SG, Binda E, Fiocco R, Vescovi AL, Shah K. Brain cancer stem cells. *Journal of molecular medicine.* 2009; 87:1087–95. [PubMed: 19784875]
20. Shackleton M, Quintana E, Fearon ER, Morrison SJ. Heterogeneity in cancer: cancer stem cells versus clonal evolution. *Cell.* 2009; 138:822–9. [PubMed: 19737509]
21. Singh SK, Hawkins C, Clarke ID, Squire JA, Bayani J, Hide T, et al. Identification of human brain tumour initiating cells. *Nature.* 2004; 432:396–401. [PubMed: 15549107]
22. Son MJ, Woolard K, Nam DH, Lee J, Fine HA. SSEA-1 is an enrichment marker for tumor-initiating cells in human glioblastoma. *Cell Stem Cell.* 2009; 4:440–52. [PubMed: 19427293]
23. Ward RJ, Lee L, Graham K, Satkunendran T, Yoshikawa K, Ling E, et al. Multipotent CD15+ cancer stem cells in patched-1-deficient mouse medulloblastoma. *Cancer Res.* 2009; 69:4682–90. [PubMed: 19487286]
24. Capela A, Temple S. LeX/ssea-1 is expressed by adult mouse CNS stem cells, identifying them as nonependymal. *Neuron.* 2002; 35:865–75. [PubMed: 12372282]
25. Patru C, Romao L, Varlet P, Coulombel L, Raponi E, Cadusseau J, et al. CD133, CD15/SSEA-1, CD34 or side populations do not resume tumor-initiating properties of long-term cultured cancer stem cells from human malignant glioma-neuronal tumors. *BMC Cancer.* 2010; 10:66. [PubMed: 20181261]
26. Piccirillo SG, Reynolds BA, Zanetti N, Lamorte G, Binda E, Broggi G, et al. Bone morphogenetic proteins inhibit the tumorigenic potential of human brain tumour-initiating cells. *Nature.* 2006; 444:761–5. [PubMed: 17151667]
27. Lee J, Kotliarova S, Kotliarov Y, Li A, Su Q, Donin NM, et al. Tumor stem cells derived from glioblastomas cultured in bFGF and EGF more closely mirror the phenotype and genotype of primary tumors than do serum-cultured cell lines. *Cancer Cell.* 2006; 9:391–403. [PubMed: 16697959]
28. Pollard SM, Yoshikawa K, Clarke ID, Danovi D, Stricker S, Russell R, et al. Glioma stem cell lines expanded in adherent culture have tumor-specific phenotypes and are suitable for chemical and genetic screens. *Cell Stem Cell.* 2009; 4:568–80. [PubMed: 19497285]
29. Danovi D, Folarin AA, Baranowski B, Pollard SM. High content screening of defined chemical libraries using normal and glioma-derived neural stem cell lines. *Methods Enzymol.* 2012; 506:311–29. [PubMed: 22341231]
30. Stupp R, Mason WP, van den Bent MJ, Weller M, Fisher B, Taphoorn MJ, et al. Radiotherapy plus concomitant and adjuvant temozolomide for glioblastoma. *N Engl J Med.* 2005; 352:987–96. [PubMed: 15758009]
31. Jansen M, Yip S, Louis DN. Molecular pathology in adult gliomas: diagnostic, prognostic, and predictive markers. *Lancet Neurol.* 2010; 9:717–26. [PubMed: 20610347]
32. Ostermann S, Csajka C, Buclin T, Leyvraz S, Lejeune F, Decosterd LA, et al. Plasma and cerebrospinal fluid population pharmacokinetics of temozolomide in malignant glioma patients. *Clin Cancer Res.* 2004; 10:3728–36. [PubMed: 15173079]

33. Portnow J, Badie B, Chen M, Liu A, Blanchard S, Synold TW. The neuropharmacokinetics of temozolomide in patients with resectable brain tumors: potential implications for the current approach to chemoradiation. *Clin Cancer Res.* 2009; 15:7092–8. [PubMed: 19861433]
34. Dietrich J, Wang D, Batchelor TT. Cediranib: profile of a novel anti-angiogenic agent in patients with glioblastoma. *Expert Opin Investig Drugs.* 2009; 18:1549–57.
35. Batchelor TT, Duda DG, di Tomaso E, Ancukiewicz M, Plotkin SR, Gerstner E, et al. Phase II study of cediranib, an oral pan-vascular endothelial growth factor receptor tyrosine kinase inhibitor, in patients with recurrent glioblastoma. *J Clin Oncol.* 2010; 28:2817–23. [PubMed: 20458050]
36. Hamerlik P, Lathia JD, Rasmussen R, Wu Q, Bartkova J, Lee M, et al. Autocrine VEGF-VEGFR2-Neuropilin-1 signaling promotes glioma stem-like cell viability and tumor growth. *J Exp Med.* 2012; 209:507–20. [PubMed: 22393126]
37. Pistollato F, Abbadi S, Rampazzo E, Persano L, Della Puppa A, Frasson C, et al. Intratumoral hypoxic gradient drives stem cells distribution and MGMT expression in glioblastoma. *Stem Cells.* 2010; 28:851–62. [PubMed: 20309962]
38. Holland EC, Celestino J, Dai C, Schaefer L, Sawaya RE, Fuller GN. Combined activation of Ras and Akt in neural progenitors induces glioblastoma formation in mice. *Nat Genet.* 2000; 25:55–7. [PubMed: 10802656]
39. Zheng H, Ying H, Yan H, Kimmelman AC, Hiller DJ, Chen AJ, et al. p53 and Pten control neural and glioma stem/progenitor cell renewal and differentiation. *Nature.* 2008; 455:1129–33. [PubMed: 18948956]
40. Wang Y, Yang J, Zheng H, Tomasek GJ, Zhang P, McKeever PE, et al. Expression of mutant p53 proteins implicates a lineage relationship between neural stem cells and malignant astrocytic glioma in a murine model. *Cancer Cell.* 2009; 15:514–26. [PubMed: 19477430]
41. Letouze E, Allory Y, Bollet MA, Radvanyi F, Guyon F. Analysis of the copy number profiles of several tumor samples from the same patient reveals the successive steps in tumorigenesis. *Genome Biol.* 2010; 11:R76. [PubMed: 20649963]
42. Yatabe Y, Tavaré S, Shibata D. Investigating stem cells in human colon by using methylation patterns. *Proc Natl Acad Sci U S A.* 2001; 98:10839–44. [PubMed: 11517339]
43. Shibata D, Tavaré S. Counting divisions in a human somatic cell tree: how, what and why? *Cell Cycle.* 2006; 5:610–4. [PubMed: 16582617]
44. Sottoriva A, Spiteri I, Shibata D, Curtis C, Tavaré S. Single-molecule genomic data delineate patient-specific tumor profiles and cancer stem cell organization. *Cancer Res.* 2013; 73:41–9. [PubMed: 23090114]
45. Lim DA, Cha S, Mayo MC, Chen MH, Keles E, VandenBerg S, et al. Relationship of glioblastoma multiforme to neural stem cell regions predicts invasive and multifocal tumor phenotype. *Neuro Oncol.* 2007; 9:424–9. [PubMed: 17622647]
46. Kappadakunnel M, Eskin A, Dong J, Nelson SF, Mischel PS, Liau LM, et al. Stem cell associated gene expression in glioblastoma multiforme: relationship to survival and the subventricular zone. *J Neurooncol.* 2010; 96:359–67. [PubMed: 19655089]
47. Ye CJ, Stevens JB, Liu G, Bremer SW, Jaiswal AS, Ye KJ, et al. Genome based cell population heterogeneity promotes tumorigenicity: the evolutionary mechanism of cancer. *J Cell Physiol.* 2009; 219:288–300. [PubMed: 19115235]
48. Stieber D, Golebiewska A, Evers L, Lenkiewicz E, Brons NH, Nicot N, et al. Glioblastomas are composed of genetically divergent clones with distinct tumorigenic potential and variable stem cell-associated phenotypes. *Acta Neuropathol.* 2014; 127:203–19. [PubMed: 24154962]
49. Sanai N, Tramontin AD, Quinones-Hinojosa A, Barbaro NM, Gupta N, Kunwar S, et al. Unique astrocyte ribbon in adult human brain contains neural stem cells but lacks chain migration. *Nature.* 2004; 427:740–4. [PubMed: 14973487]
50. Sanai N, Alvarez-Buylla A, Berger MS. Neural stem cells and the origin of gliomas. *N Engl J Med.* 2005; 353:811–22. [PubMed: 16120861]
51. Evers P, Lee PP, DeMarco J, Agazaryan N, Sayre JW, Selch M, et al. Irradiation of the potential cancer stem cell niches in the adult brain improves progression-free survival of patients with malignant glioma. *BMC Cancer.* 2010; 10:384. [PubMed: 20663133]

52. Chen L, Guerrero-Cazares H, Ye X, Ford E, McNutt T, Kleinberg L, et al. Increased subventricular zone radiation dose correlates with survival in glioblastoma patients after gross total resection. *Int J Radiat Oncol Biol Phys.* 2013; 86:616–22. [PubMed: 23540348]

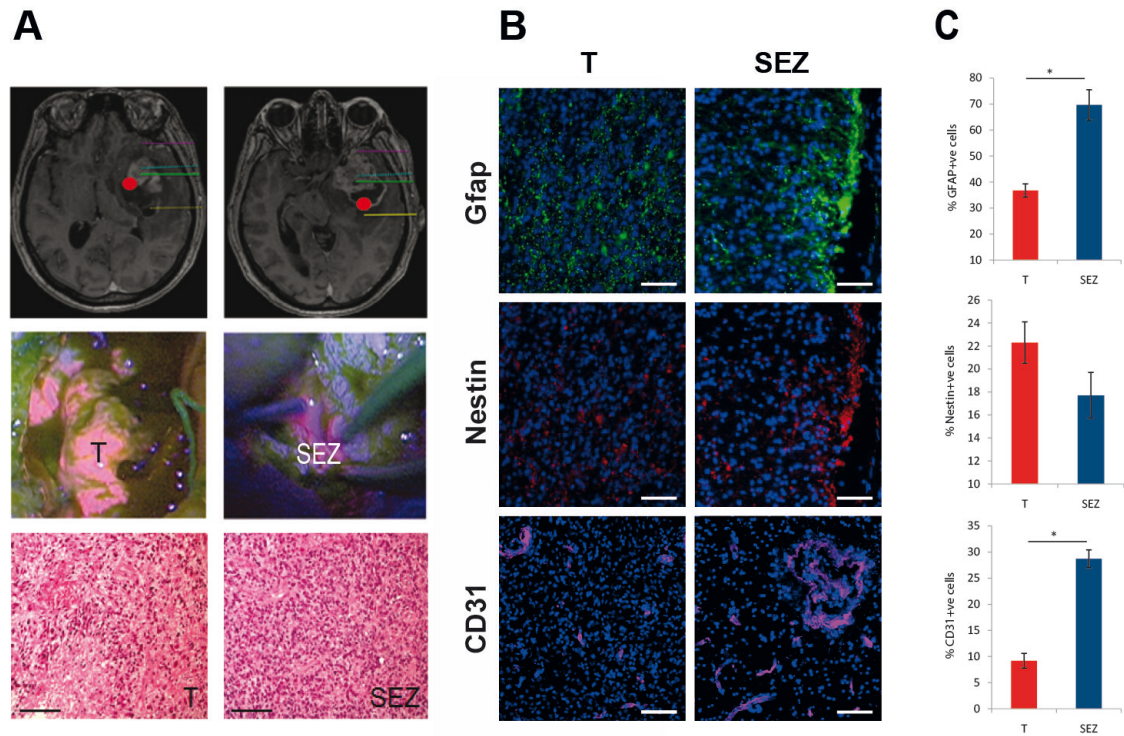


Figure 1. Identification of SEZ in human GB

(A) Top panel. Illustrative MRI scans of a GB in the right temporal lobe. Red dots indicate tissue sampling from T and SEZ. **Middle panel.** Peri-operative images of visible fluorescence from T and SEZ indicating the presence of tumor tissue. **Bottom panel.** Haematoxylin&Eosin staining of T and SEZ. Both show cardinal features of GB (high mitotic index, nuclear atypia, mitosis and microvascular proliferation). Scale bar, 100 μ m. **(B)** T and SEZ tissues have been stained for Gfap (green), Nestin (red), CD31 (pink) and counterstained with DAPI (blue). SEZ is characterized by Gfap expression and high vascularization. Scale bar, 100 μ m. **(C)** Quantitative analysis of Gfap-, Nestin- and CD31-positive cells in T and SEZ tissues of the same patient.

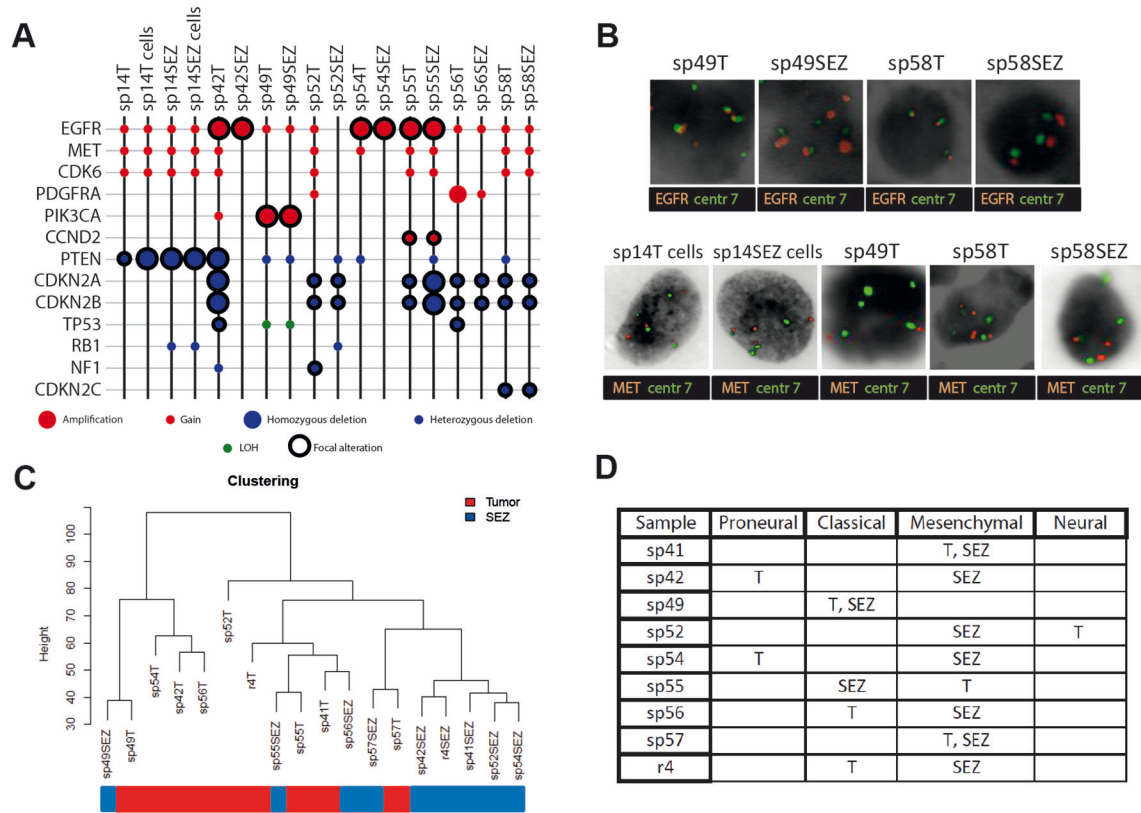


Figure 2. The SEZ harbors residual disease

(A) Summary of the most common putative drivers in GB. In 6/8 patients the SEZ contains an equal or smaller number of aberrations with respect to its corresponding T. Cultured cells from T and SEZ of patient sp14 have been used for comparison with the corresponding tissues. (B) FISH of 3 patients confirms gain of the region of chromosome 7 including EGFR and the centromere (centr 7) in sp49 and sp58 (T and SEZ in both cases) and gain of the region including MET and centr 7 in sp58 and cells from sp14 (T and SEZ in both cases); as expected, based on copy number data, gain of MET was not observed in sp49T. Orange denotes EGFR or MET and green the centr 7. The single nuclei are representative of what was generally observed in each sample. (C) Clustering of gene expression profiles from 9 patients reveals that 5 SEZ samples cluster tightly together instead of with their matched T. Samples are color-coded based on their origin. (D) Each compartment of 9 GBs has been assigned to a previously described classifier (6): T samples are either Proneural, Classical, Mesenchymal or Neural and 7/9 SEZ are Mesenchymal.

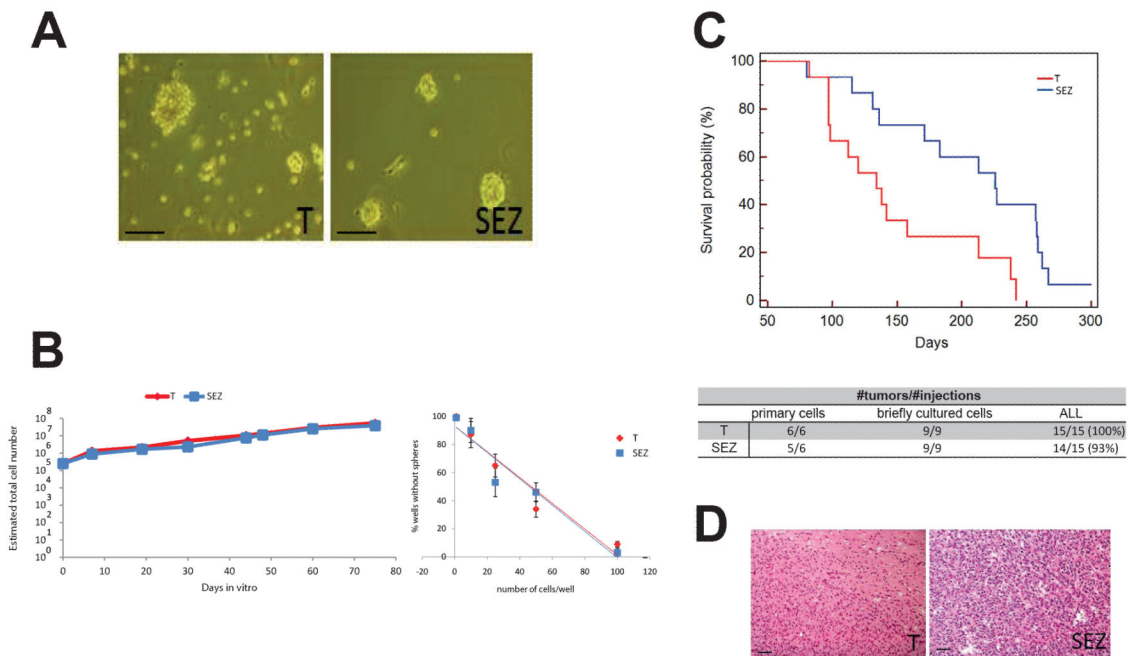


Figure 3. TICs can be isolated from SEZ of GB patients

(A) Cells from T and SEZ form spheres in serum-free medium. Magnification 100 \times ; scale bar 50 μ m. (B) **Left.** Growth curve analysis shows that cells from T and SEZ are capable of long-term expansion. **Right.** Limiting-dilution assays reveal similar frequencies of sphere-formation in T and SEZ. Each data point represents the average of triplicates. Error bars, s.d. (C) **Top.** Cumulative Kaplan-Meier survival analysis of 30 animals reveals the tumorigenic potential of T and SEZ cells from 5 GBs. There is a statistically significant difference (p -value <0.05, Logrank test) between the survival of animals injected with T cells *versus* those injected with SEZ cells. **Bottom.** Table summarizing the number of tumors/injections and the type of cells used (primary or briefly cultured). (D) Haematoxylin&Eosin staining of T and SEZ cells-derived xenografts. Scale bar, 30 μ m.

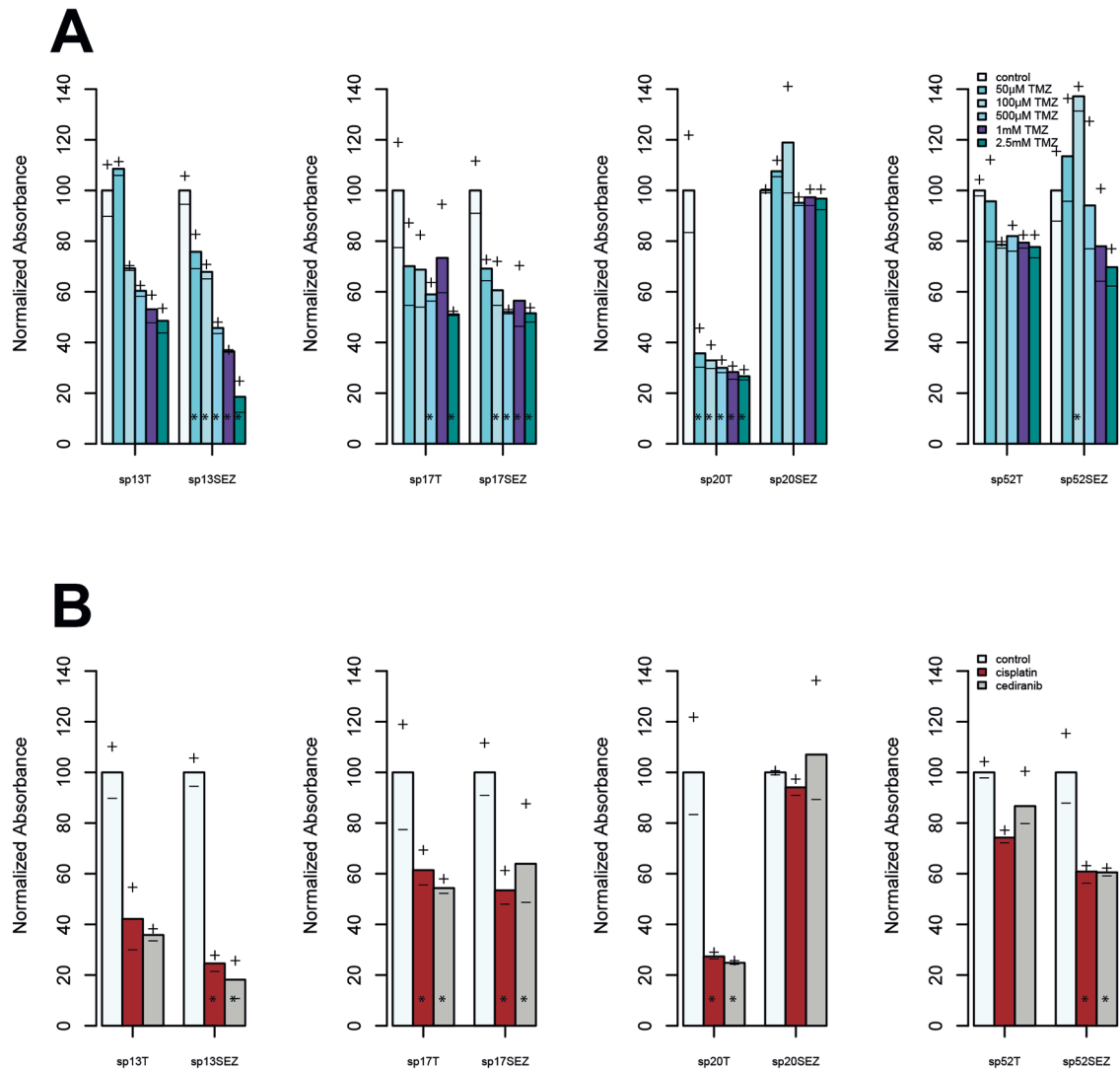


Figure 4. TICs from SEZ contribute to drug resistance

Cells from T and SEZ of 4 patients were used to evaluate response to chemotherapeutics. **(A)** Differential response patterns to temozolomide (TMZ) were observed in T and SEZ cells of the same patients. Dose escalation has little impact on drug-resistant cells. **(B)** Distinct patterns of response are observed when the assay is performed with Cisplatin and Cediranib. Data are shown as normalized to control. The mean normalized absorbance as well as the minimum (-) and maximum (+) absorbance are plotted. Asterisks indicate statistical significance.

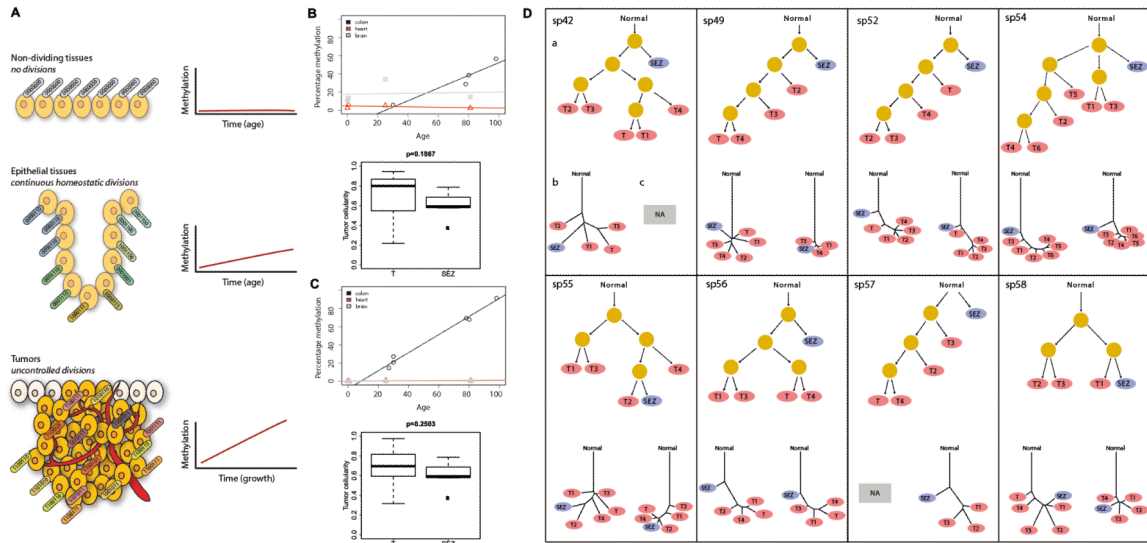


Figure 5. Phylogenetic reconstruction reveals different patterns of tumor evolution involving SEZ malignant cells

(A) Cartoon illustrating the phylogeny based on molecular clock analysis. Non-dividing tissues, such as heart and brain, do not undergo mitotic events and do not accumulate methylation errors. Epithelial tissues, such as colon, show increased methylation with age due to the mitotic turnover of cells maintaining tissue homeostasis. Tumors undergo a large number of divisions and accumulate methylation changes in a manner proportional to the number of mitotic events. (B, C) **Top.** The IRX2 locus on chromosome 5 (in B) and the NETO1 locus on chromosome 18 (in C) have been validated as molecular clock loci by verifying that age-related methylation increases as a result of cell division in patient-derived tissues by comparing heart, brain and colon. **Bottom.** The graphs show tumor cellularity using IRX2 (in B) and NETO1 (in C) molecular clock data. The values of cellularity indicate no significant difference between T and SEZ. (D) Tumor phylogenies based on SEZ and multiple tumor mass samples (T, T1-T6) were reconstructed independently with 2 methods: copy number breakpoints (a) and two molecular clock loci (b, IRX2 and c, NETO1). As an example, in sp52 the SEZ (blue) harbors cells that arise earlier than tumor mass cells (red) (sample T1 failed hybridization). NA= not available.